Spin-correlation imaging of electrons in ferromagnets

A. Morozov, J. Berakdar, S. N. Samarin, F. U. Hillebrecht, and J. Kirschner
Max-Planck-Institut für Mikrostrukturphysik, Weinberg 2, 06120 Halle, Germany
(Received 27 August 2001; published 26 February 2002)

The angular and energy dependencies of the exchange interaction between the electrons in an itinerant ferromagnetic surface can be mapped out by exciting two interacting spin-polarized electrons into the vacuum and resolving at the same time the energies and emission angles of the two electrons. From a tensorial symmetry analysis it is deduced that the recorded two-particle spectra carry detailed information on the spin-split electronic structure that can be extracted under favorable conditions. To substantiate these statements we present and analyze experimental results and numerical calculations for a ferromagnetic iron surface.

DOI: 10.1103/PhysRevB.65.104425 PACS number(s): 75.30.Ds, 34.80.Nz, 34.80.Dp, 79.20.Kz

I. INTRODUCTION

The fermionic nature of electrons dictates that the quantum-mechanical wave function of a multielectron system has to be antisymmetric with respect to exchange of the states of two individual electrons. This symmetry requirement has profound consequences as to the properties of correlated electronic systems. In particular, the exchange ''coupling'' between electrons is essential for the ferromagnetic state of matter. Therefore, experimental and theoretical approaches that expose details of the energy and angular dependencies of the exchange interaction are of considerable value for fundamental and applied research. The obstacles encountered in such studies are of a technical as well as of a theoretical/conceptual nature: To investigate the influence of the exchange interaction one should be able to control experimentally the states, i.e., the quantum numbers, of at least two electrons and then change the spin state of one of these electrons while monitoring the change in the properties of the system.

Experimentally, this can be realized by measuring the two-particle excitation spectrum of a ferromagnet upon the impact of a single polarized electron. Features related to the exchange interaction are studied by observing the dependence of the spectrum on the electrons' spin projections. It is clear from the outset that such measurements put high demands on the experiment as one has to utilize a multiparticle coincidence technique using a spin-polarized beam to resolve and control the two electrons' quantum numbers. Such a method is hampered by low counting rates as compared to conventional single-particle spectroscopic techniques. Nevertheless, since the exchange coupling is a many-body effect it is indispensable to use many-particle techniques to trace the various facets of this interaction, such as the energy and angular dependencies of the exchange-influenced pair-correlation function. Correspondingly, a theoretical treatment has to deal with the excited states of a fermionic many-body system to describe the propagation of two hot electrons that interact with each other and with the surface and emerge eventually into the vacuum with well-defined wave vectors and with a given total spin of the electron pair.

The experimental approach used in this work can be regarded as an extension of the well-established spin-polarized electron energy-loss spectroscopy (SPEELS) as applied to the study of the electron-hole pair excitations in ferromagnets, known as the Stoner spectrum.[1–5] The Stoner excitation of a ferromagnetic surface involves a two-state transition: A majority band electron interacts with the incoming polarized electron (of opposite spin projection) and is promoted to a highly excited state. If this state lies above the vacuum level, the electron may escape such that it can be detected by a suitable detector. Due to this interaction, the projectile electron loses energy and relaxes into an unoccupied (hot-electron) state in the minority band. Therefore, an observer monitoring the spin state and the energy loss of the incoming polarized electron beam registers (using SPEELS) a spin-flip event at a certain energy loss determined by the characteristics of the unoccupied density of states of the minority band. In a SPEELS experiment only one (the excited majority band electron) is detected while the mechanism that triggered the transition is an exchange process that involves, at least, two electrons. To map out the details of the exchange-dependent electron-electron scattering one needs to resolve the energies and emission angles of the two electrons which are excited upon the interaction of one single energetic, spin-polarized electron with a single domain ferromagnet. The dependence of the spectrum on the spin projection of the projectile electron and/or the magnetization direction of the sample yields direct information on the spin-dependent electronic interactions. If spin-orbit interactions are deemed small it suffices to determine the spin states of the electrons prior to the collision as the total spin is conserved (this does not exclude the possibility for the individual electrons to exchange their spin projections via exchanging their energies and emission angles. The latter exchange process is mediated by the spin-independent electron-electron interaction).

In this work we conducted this type of experiment on an Fe(110) single-crystal surface with a well-defined magnetization direction. The experiment allows one to set the energy and spin polarization of the incoming electron beam. The measurement determines the energy and angle-resolved coincidence rate of electron pairs emitted after excitation by a single electron. Furthermore, in order to address the influence of the exchange interaction directly, the relative orientation of sample magnetization and incident-beam polarization is switched between parallel and antiparallel.

As deduced from a tensorial symmetry analysis, the spin-dependent two-particle spectrum can be classified according

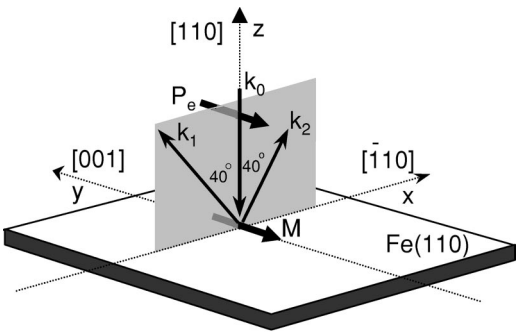

FIG. 1. The experimental setup as used for the coincidence measurements. The direction of the magnetization **M**, the spin-polarization vector of the incoming beam $\mathbf{P}_1$, as well as the wave vectors of the incoming and the two emitted electrons $\mathbf{k}_0$ and $\mathbf{k}_1$, $\mathbf{k}_2$ are indicated. The electron detectors are positioned at 40° to the left and to the right of the *z* axis.

to the symmetry of the interactions involved in the excitation process (exchange and spin-orbit interactions). The mathematical treatment yields a prescription to disentangle and measure the various terms related to a specific symmetry class. For the calculations of the two-particle spectrum we utilize a numerical method which employs a realistic spin-split surface electronic band structure combined with a Green-function technique to propagate the two excited, correlated electrons into the vacuum in the presence of the scattering from the surface crystal potential.

The results of this work show a strong dependence of the two-electron coincidence signal on the direction of the spin polarization of the incoming beam. The origin of this spin asymmetry is revealed by an analysis of its rotational properties (in the two-electron spin space). From this analysis we conclude that, within the resolution of the present setup, the spin asymmetry measured for the Fe(110) surface is induced by the exchange coupling. It depends on the mutual angle of the two escaping electrons as well as on their relative energies and on the crystal orientation, providing thus detailed information on the influence of the exchange interaction on excited electrons at surfaces. A brief account of the present studies and first results has been published in Refs. 6 and 7.

II. EXPERIMENTAL DETAILS

The experimental realization of the coincident measurement is depicted in Fig. 1. A pulsed spin-polarized electron beam with wave vector $\mathbf{k}_0$ impinges onto a clean ferromagnetic surface, in our study, bcc Fe(110). The time structure in combination with the very low average current of the incoming beam ensure that only single electrons interact with the sample. A fraction of the scattering events leads to the emission of two electrons with energies E_1, E_2 and emission angles θ_1, θ_2 with respect to the incoming beam direction.

Hence, the experiment measures simultaneously the wave vectors $\mathbf{k}_0$ and $\mathbf{k}_1$, $\mathbf{k}_2$ of the impinging and two ejected electrons. The escaping electrons are detected by two position sensitive time-of-flight (TOF) detectors. The sample normal, the incident electron beam, and the axes of the TOF detectors are in the same plane. The polarization vector $\mathbf{P}_1$ of the incident beam and the magnetization direction of the sample are both perpendicular to the scattering plane (cf. Fig. 1). As a source of spin-polarized electrons we used a strained GaAs multilayer photocathode activated by Cs deposition and oxygen exposure. Photoelectrons generated from the photocathode by the circularly polarized light of a laser diode are deflected by a 90° deflector to convert the longitudinally polarized beam into a transversely polarized one. At an electron pulse frequency of 500 MHz, the average coincidence count rate was 30 events per s. To obtain a data set with statistics suitable for the detailed analysis presented in this paper, a typical spectrum took an acquisition time of about 100 h. This long term measurement requires good vacuum conditions to maintain a clean sample surface, and good stability of the incident-beam polarization. To reduce the influence of the possible instabilities the polarization of the incident beam is inverted every 5 s and the data for each polarization are stored in two different files. In spite of the UHV conditions ($\approx 5.10^{-11}$ mbar) the cleanliness of the sample surface has to be restored regularly. This was done by Ar^+ ion sputtering followed by annealing and, if necessary, oxygen treatment to remove the carbon from the surface. The surface properties were monitored by Auger electron spectroscopy and low-energy electron diffraction. The experiment requires a high degree of polarization of the incident beam and single domain magnetization of the sample. To monitor these conditions we measured the energy-loss spectra (the Stoner spectrum) for an electron-beam polarization parallel and antiparallel to the magnetization in the same geometry of Fig. 1 with one of the TOF detectors switched off.[8] The asymmetry *A*, derived from the two intensities for the opposite spin projections of the incident beam, is measured before and after the coincidence experiments and is used as an indicator for the stability of the experimental setup.

The energy and wave-vector balance imposes the conditions

$$E_0 + \epsilon = E_1 + E_2, \tag{1}$$

$$\mathbf{k}_{0\parallel} + \mathbf{q}_\parallel + \mathbf{g}_\parallel = \mathbf{k}_{1\parallel} + \mathbf{k}_{2\parallel}. \tag{2}$$

Here, ϵ is the energy of the valence-band electron and $\mathbf{q}_\parallel$ is its (surface) Bloch wave vector. The surface reciprocal-lattice vector is denoted by $\mathbf{g}_\parallel$. Since the quantities E_0, E_1, and E_2 and $\mathbf{k}_0$, $\mathbf{k}_{1\parallel}$, and $\mathbf{k}_{2\parallel}$ are determined experimentally (cf. Fig. 1) we can control, via Eqs. (1) and (2), the values of ϵ and $\mathbf{q}_\parallel$, i.e., we can perform the experiment in a certain region of the (magnetic) surface Brillouin zone. Lowering E_2 while keeping E_1 and E_0 fixed we can zoom in to deeper levels of the conduction band. Equivalently, one can scan $\mathbf{q}_\parallel$ by varying, e.g., $\mathbf{k}_{0\parallel}$ for given $\mathbf{k}_{1\parallel}$, $\mathbf{k}_{2\parallel}$, and $\mathbf{g}_\parallel$. The experiment (Fig. 1) measures a spin asymmetry $\mathcal{A}$, i.e., for a certain magnetization direction **M**, hereafter denoted by $\Downarrow^{\mathrm{M}}$, we register the electron-pair emission rate *W* for antiparallel and parallel alignment of the polarization vector of the incoming beam with **M** (cf. Fig. 1) and evaluate $\mathcal{A}$ as

$$\mathcal{A}(\mathbf{k}_1,\mathbf{k}_2;\mathbf{k}_0)=\frac{W(\uparrow\Downarrow^{\mathrm{M}})-W(\downarrow\Downarrow^{\mathrm{M}})}{W(\uparrow\Downarrow^{\mathrm{M}})+W(\downarrow\Downarrow^{\mathrm{M}})}. \tag{3}$$

III. THEORETICAL CONSIDERATIONS

For a theoretical formulation we describe the incoming polarized electron beam as a (microcanonical) ensemble and quantify it by the density operator ρ^{s_1} with matrix elements $\rho^{s_1}_{m_{s_1}m_{s_1}}$. Here m_{s_1} is the projection of the electron's spin $\mathbf{s}_1$ along an appropriately chosen quantization axis (e.g., the magnetization direction). The density matrix is chosen to be diagonal. This is not a restriction since it can always be diagonalized by an appropriate unitary transformation. In the standard representation the density operator ρ^{s_1} is expanded linearly in terms of the Pauli matrices σ as

$$\rho^{s_1}=\mathbf{1}+\mathbf{P}_1\cdot\sigma, \tag{4}$$

where $\mathbf{P}_1$ is the polarization vector of the beam. Analogously, the electrons in the exchange-split conduction band are characterized by the density matrix $\overline{\rho}^{s_2}_{m_{s_2}m_{s_2}}$ where s_2 is the spin of the electron and m_{s_2} labels the corresponding magnetic sublevels. The density operator $\overline{\rho}^{s_2}$ is expressed as

$$\overline{\rho}^{s_2}=w_0(\mathbf{k}_{2\parallel},l,\epsilon)(\mathbf{1}+\mathbf{P}_2\cdot\sigma), \tag{5}$$

where $w_0(\mathbf{k}_{2\parallel},l,\epsilon)$ is the spin-averaged Bloch spectral function of the layer l and $\mathbf{P}_2$ characterizes the polarization of the band states, for its value is defined as

$$P_2=\frac{w(\mathbf{k}_{2\parallel},l,\epsilon,\Uparrow)-w(\mathbf{k}_{2\parallel},l,\epsilon,\Downarrow)}{w_0(\mathbf{k}_{2\parallel},l,\epsilon)}. \tag{6}$$

Here $w(\mathbf{q}_\parallel,l,\epsilon,\Uparrow)$ and $w(\mathbf{q}_\parallel,l,\epsilon,\Downarrow)$ are the Bloch spectral functions of, respectively, the majority and the minority bands. The spin-averaged Bloch spectral function is denoted by w_0. These samples' spectral functions are obtained from the trace of the imaginary part of the corresponding single-particle Green function of the surface. For the calculations of the (ground-state) electronic properties of the sample we utilized the full-potential linearized augmented plane-wave method[9] and compared the results with those obtained from a self-consistent layer-resolved Korringa-Kohn-Rostoker method.[10] Both methods are based on density-functional theory within the local-density approximation. The density matrix ρ^S of the combined electron-surface system, long before the collision, is obtained from the direct product $\rho^S=\rho^{s_1}\otimes\overline{\rho}^{s_2}$.

For the calculations of the pair-emission probability we note that the experiment resolves the asymptotic wave vectors of the impinging and the two emitted (vacuum) electrons (cf. Fig. 1). However, no spin analysis of the outgoing electrons is performed in the final channel. Such a spin analysis is redundant in the absence of spin-orbit interaction, as shown below.

The cross section W for the simultaneous emission of two electrons with wave vectors $\mathbf{k}_1$ and $\mathbf{k}_2$ in response to the impact of a projectile electron with wave vector $\mathbf{k}_0$ is given by

$$W(\mathbf{k}_2,\mathbf{k}_1;\mathbf{k}_0)=C\sum_{\substack{m_{s_1'},m_{s_2'}\\ m_{s_1},m_{s_2}}}\oint_\alpha T\rho^S T^\dagger\delta(E_f-E_i). \tag{7}$$

Here $m_{s_1'},m_{s_2'}$ denote the spin projections of the final-state electrons and α stands for all the quantum numbers needed to quantify uniquely the quantum-mechanical state of the system which are not resolved by the experiment. $C=(2\pi)^4/k_0$ is a kinematical factor that originates from the normalization to the incoming electron flux current density.

In Eq. (7) T denotes the matrix elements of the transition operator $\mathcal{T}$ of the total system consisting of the projectile electron and the magnetic surface, i.e.,

$$T(\mathbf{k}_1,m_{s_1'},\mathbf{k}_2,m_{s_2'};\mathbf{k}_0,m_{s_1},\alpha,m_{s_2})=\langle\psi_{\mathbf{k}_1,\mathbf{k}_2,m_{s_1'},m_{s_2'}}(1,2)|\mathcal{T}|\phi_{\epsilon,\alpha,s_2,m_{s_2}}(2)\varphi_{\mathbf{k}_0,s_1m_{s_1}}(1)\rangle. \tag{8}$$

$\varphi_{\mathbf{k}_0,s_1m_{s_1}}$ is a spinor vacuum state describing the incoming beam. The ground state of the surface is to be described by the single-particle, spin-resolved orbital $\phi_{\epsilon,\alpha,s_2,m_{s_2}}(2)$ which is characterized by the energy ϵ, the spin state s_2,m_{s_2}, and the collective quantum numbers α. The emitted electrons with spin projections $m_{s_1'},m_{s_2'}$ are represented by the two-particle state vector $|\psi_{\mathbf{k}_1,\mathbf{k}_2,m_{s_1'},m_{s_2'}}(1,2)\rangle$.

To leading order in the electron-electron and the electron-crystal interaction the operator $\mathcal{T}$ can be approximated by[11] $\mathcal{T}\approx U_{surf}+U_{ee}(\mathbf{1}+G^-_{ee}U_{surf})$ where U_{ee} is the electron-electron interaction, G^-_{ee} is the Green function within the potential U_{ee}, and U_{surf} is the surface scattering potential. For a given atomic layer of the surface the potential U_{surf} is cast in a nonoverlapping muffin-tin form. For the electronic interaction U_{ee} we employ a screened Coulomb potential with the screening length determined according to the Thomas-Fermi theory. In T we discard any spin-orbit effects. The justification for the neglect of spin-orbit interaction can be checked experimentally, as explained below.

A. Tensorial recoupling

Having sketched the general calculational scheme it is advantageous to analyze the transformational properties of the spectrum (7) using group theory. This analysis is generally valid and does not rely on the specific approximation to $\mathcal{T}$. To this end and to disentangle geometrical from dynamical features we express the density matrices (4) and (5) in terms of the statistical tensors $\rho_{p_1q_1}$ and $\overline{\rho}_{p_2q_2}$,[12]

$$\rho^{s_1}_{m_{s_1}m_{s_1}} = \sum_{p_1=0}^{2s_1} (-)^{p_1-s_1-m_{s_1}} \times \langle s_1 - m_{s_1}; s_1 m_{s_1} | p_1 q_1 = 0 \rangle \rho_{p_1 q_1 = 0}, \quad (9)$$

$$\overline{\rho}^{s_2}_{m_{s_2}m_{s_2}}(\epsilon,\alpha) = \sum_{p_2=0}^{2s_2} (-)^{p_2-s_2-m_{s_2}} \times \langle s_2 - m_{s_2}; s_2 m_{s_2} | p_2 q_2 = 0 \rangle \overline{\rho}_{p_2 q_2 = 0}(\epsilon,\alpha). \quad (10)$$

We recall here that the density matrices are both diagonal due to the assumption that there exists a common quantization axis, therefore, only the components along the axes $\rho_{p_1 q_1=0}$ and $\overline{\rho}_{p_2 q_2=0}$ appear in Eqs. (9) and (10) [in Eqs. (9) and (10) $\langle \cdots | \cdots \rangle$ denotes Clebsch-Gordon coefficients].

Substituting Eqs. (9) and (10) into the general expression (7) yields

$$W = \sum\!\!\!\!\!\!\int_{\alpha} \sum_{p_1=0}^{2s_1} \sum_{p_2=0}^{2s_2} \rho_{p_1 q_1=0} \overline{\rho}_{p_2 q_2=0}(\epsilon,\alpha) \Lambda^{p_1,p_2}_{q_1=0,q_2=0} \times \delta(E_f - E_i), \quad (11)$$

where

$$\Lambda^{p_1,p_2}_{q_1=0,q_2=0} = \sum_{m_{s_1}} (-)^{p_1-s_1-m_{s_1}} \langle s_1 - m_{s_1}; s_1 m_{s_1} | p_1 q_1 = 0 \rangle \times \sum_{m_{s_2}} (-)^{p_2-s_2-m_{s_2}} \langle s_2 - m_{s_2}; s_2 m_{s_2} | p_2 q_2 = 0 \rangle \times \mathcal{F}_{\alpha}(m_{s_1}, m_{s_2}), \quad (12)$$

$$\mathcal{F}_{\alpha}(m_{s_1},\alpha,m_{s_2}) = C \sum_{\substack{m_{s_1'} \\ m_{s_2'}}} T(\mathbf{k}_1, m_{s_1'}, \mathbf{k}_2, m_{s_2'}; \mathbf{k}_0, m_{s_1}, \alpha, m_{s_2}) \times T^{\dagger}(\mathbf{k}_1, m_{s_1'}, \mathbf{k}_2, m_{s_2'}; \mathbf{k}_0, m_{s_1}, \alpha, m_{s_2}). \quad (13)$$

The complete dynamical information on the two-particle emission are encompassed in $\Lambda^{p_1,p_2}_{q_1,q_2}$ whereas the geometry of the ground state is described by the state multipoles.

The importance of the above recoupling scheme follows from the conclusion that the sum over m_{s_1} (m_{s_2}) in Eq. (13) defines the component along the quantization axis (the magnetization direction) of a spherical tensor of rank p_1 (p_2) while the dependence of the sum on $m_{s_1'}$ ($m_{s_2'}$) is considered parametrically. This is readily deduced from the fact that for given spin projections $m_{s_1'}$ and $m_{s_2'}$ the m_{s_1} (m_{s_2}) behavior of T is given by the dependence on the magnetic sublevels of an angular momentum state, namely, by the m_{s_1} (m_{s_2}) dependence of the spin part of $|\varphi_{\mathbf{k}_1,s_1 m_{s_1}}(1)\rangle$ $[|\phi_{\epsilon,\alpha,s_2,m_{s_2}}(2)\rangle]$. Thus $T(\mathbf{k}_1, m_{s_1'}, \mathbf{k}_2, m_{s_2'}; \mathbf{k}_0, m_{s_1}, \alpha, m_{s_2})$ may be regarded as the m_{s_1} (m_{s_2}) component of a spherical tensor of rank s_1 (s_2). Furthermore, the complex conjugate can be written in the form $T^*(s_1, m_{s_1}) = (-)^{\delta - m_{s_1}} \mathcal{W}(s_1, -m_{s_1})$. This relation is a definition for the tensor $\mathcal{W}$, and resembles formally the definition of the adjoint of a tensor operator where the phase δ is chosen arbitrarily under the constraint that $\delta - m_{s_1}$ must be an integer.[13] Thus we choose $\delta - m_{s_1} = p_1 - s_1 - m_{s_1}$ (note that $p_1 = 0 \cdots 2s_1$ and $s_1 - m_{s_1}$ are always integers). The tensor product of $T(s_1, m_{s_1})$ and $T^{\dagger}(s_1, m_{s_1})$, which is again a spherical tensor, is then given by

$$[T(s_1, m_{s_1}) \wedge T^{\dagger}(s_1, m_{s_1})]^{p_1}_{q_1=0} = \sum_{m_{s_1}} (-)^{p_1-s_1-m_{s_1}} \langle s_1 - m_{s_1} s_1 m_{s_1} | p_1 0 \rangle \times \mathcal{W}(s_1, -m_{s_1}) T(s_1, m_{s_1}).$$

Comparing this result with Eq. (13) it is obvious that for a given p_2 the parameter $\Lambda^{p_1,p_2}_{q_1=0,q_2=0}$ can be regarded as the component along the quantization axis of a spherical tensor of rank p_1. The same argument applies to the dependence on p_2, i.e., for a given p_1 we can treat $\Lambda^{p_1,p_2}_{q_1=0,q_2=0}$ as the $\hat{\mathbf{M}}$ component of the spherical tensor with rank p_2.

This mathematical analysis yields important information as to the transformation behavior of the tensorial components $\Lambda^{p_1,p_2}_{0,0}$: $\Lambda^{p_1=0,p_2}_{0,0}$ ($\Lambda^{p_1,p_2=0}_{0,0}$) is a *scalar* with respect to spin rotations generated by $\mathbf{s}_1$ ($\mathbf{s}_2$), i.e., it represents spin-averaged quantities in the $\mathbf{s}_1$ ($\mathbf{s}_2$) spin space, whereas the components $\Lambda^{p_1=odd,p_2}_{0,0}$ ($\Lambda^{p_1,p_2=odd}_{0,0}$) can be regarded as spin *orientation* in the $\mathbf{s}_1$ ($\mathbf{s}_2$) spin space (for $p_1=1$ it is a vector) and hence changes sign upon spin reflection, i.e., $\Lambda^{p_1=odd,p_2}_{0,q_0}(-m_{s_1}) = -\Lambda^{p_1=odd,p_2}_{0,0}(m_{s_1})$ $[\Lambda^{p_1,p_2=odd}_{0,q_0}(-m_{s_2}) = -\Lambda^{p_1,p_2=odd}_{0,0}(m_{s_2})]$. The tensorial components with even p_1 values are alignment parameters, i.e., they describe the deviations in the spectra from the unpolarized case.

For the case $s_1 = 1/2$ and $s_2 = 1/2$ Eq. (11) reduces to

$$W = \sum\!\!\!\!\!\!\int_{\alpha} \left\{ \Lambda^{0,0}_{0,0} \left[\rho_{00}\overline{\rho}_{00} + \rho_{00}\overline{\rho}_{10}\frac{\Lambda^{0,1}_{0,0}}{\Lambda^{0,0}_{0,0}} + \rho_{10}\overline{\rho}_{00}\frac{\Lambda^{1,0}_{0,0}}{\Lambda^{0,0}_{0,0}} + \rho_{10}\overline{\rho}_{10}\frac{\Lambda^{1,1}_{0,0}}{\Lambda^{0,0}_{0,0}} \right] \delta(E_f - E_i) \right\}. \quad (14)$$

As stated above, the first term of the sum in Eq. (14) yields the pair-emission rate averaged over the spin orientation of the incoming electron beam and the spin polarization of the sample. The second term describes the spin asymmetry due to the inversion of the magnetization while the incoming electron beam is *unpolarized* . The third term is the spin asymmetry in the electron-pair emission from *unpolarized targets* when inverting the spin polarization of the electron beam.[14] In the absence of explicit spin interactions in the

transition operator $\mathcal{T}$, e.g., spin-orbit coupling, the parameters $\Lambda^{1,0}_{0,0}$ and $\Lambda^{0,1}_{0,0}$ vanish. In the present experiment on the Fe(110) sample we measured the parameters $\Lambda^{0,1}_{0,0}$ and $\Lambda^{1,0}_{0,0}$ and found them to be zero in the particular geometry of Fig. 1 and within the accuracy of our setup. In this context we note that with the same setup it has been possible to determine a finite value of $\Lambda^{1,0}_{0,0}$ when a tungsten sample is employed,[15] due to the enhanced strength of spin-orbit interaction as compared to the case of Fe(110).

Therefore, the present study is devoted to the last term of Eq. (14). This parameter is relevant for the description of the electron-pair emission from an exchange-split ferromagnetic surface induced by spin-polarized electrons. $\Lambda^{1,1}_{0,0}$ is a polar vector both in the $\mathbf{s}_1$ and $\mathbf{s_2}$ spin spaces, i.e.,

$$\Lambda^{1,1}_{0,0}(-m_{s_1},m_{s_2})=-\Lambda^{1,1}_{0,0}(m_{s_1},m_{s_2}),$$

$$\Lambda^{1,1}_{0,0}(m_{s_1},-m_{s_2})=-\Lambda^{1,1}_{0,0}(m_{s_1},m_{s_2}),$$

$$\Lambda^{1,1}_{0,0}(-m_{s_1},-m_{s_2})=\Lambda^{1,1}_{0,0}(m_{s_1},m_{s_2}). \tag{15}$$

The explicit forms of $\Lambda^{1,1}_{0,0}$ and $\Lambda^{0,0}_{0,0}$ are derived from Eq. (13) to be

$$\Lambda^{1,1}_{0,0}=\frac{1}{2}\{\mathcal{F}(\downarrow,\Downarrow)+\mathcal{F}(\uparrow,\Uparrow)-\mathcal{F}(\uparrow,\Downarrow)-\mathcal{F}(\downarrow,\Uparrow)\}, \tag{16}$$

$$\Lambda^{0,0}_{0,0}=\frac{1}{2}\{\mathcal{F}(\downarrow,\Downarrow)+\mathcal{F}(\uparrow,\Uparrow)+\mathcal{F}(\uparrow,\Downarrow)+\mathcal{F}(\downarrow,\Uparrow)\}. \tag{17}$$

To expose the symmetry properties of the total wave function that are imposed by the Pauli principle we transform $\mathcal{F}$ and T, as given by Eq. (8), into the total-spin (S) space and obtain (we assume separable spin and spatial degrees of freedom)

$$\mathcal{F}(m_{s_1},m_{s_2})=C\sum_{SM_S}|\langle s_1 m_{s_1};s_2 m_{s_2}|SM_S\rangle|^2 \times X^{(S)}(\mathbf{k}_1,\mathbf{k}_2;\mathbf{k}_0,\alpha), \tag{18}$$

$$X^{(S)}(\mathbf{k}_1,\mathbf{k}_2;\mathbf{k}_0,\alpha)=|\langle\Psi^{(S)}_{\mathbf{k}_1,\mathbf{k}_2}(1,2)\chi_{SM_S}(1,2)|\mathcal{T}| \times\Phi(S)(1,2)\chi'_{SM_S}(1,2)\rangle|^2. \tag{19}$$

Here we introduced the total-spin-resolved cross section $X^{(S)}$ and the normalized two-particle spin wave function as $|\chi'_{SM_S}\rangle$. The spatial parts of the two-electron state in the initial and the final channels are denoted by, respectively, $|\Psi^{(S)}_{\mathbf{k}_1,\mathbf{k}_2}(1,2)\rangle$ and $|\Phi(S)(1,2)\rangle$, i.e.,

$$|\Psi^{(S)}_{\mathbf{k}_1,\mathbf{k}_2}(1,2)\rangle=\frac{1}{\sqrt{2}}\{|\psi_{\mathbf{k}_1,\mathbf{k}_2}(1,2)\rangle+(-)^S|\psi_{\mathbf{k}_2,\mathbf{k}_1}(1,2)\rangle\}. \tag{20}$$

From this relation we deduce an important feature of the triplet state ($S=1$) and the corresponding triplet transition amplitude: In cases where an exchange of $\mathbf{k}_1$ and $\mathbf{k}_2$ does not affect the experiment, e.g., when $\mathbf{k}_1=\mathbf{k}_2$, the triplet scattering vanishes.

To understand the polarized multielectron emission it is useful to introduce the direct- (f) and the exchange- (g) scattering amplitudes. These are defined as

$$f=\langle\psi_{\mathbf{k}_1,\mathbf{k}_2}(1,2)|\mathcal{T}|\phi_{\epsilon,\alpha}(2)\varphi_{\mathbf{k}_0}(1)\rangle, \tag{21}$$

$$g=\langle\psi_{\mathbf{k}_2,\mathbf{k}_1}(1,2)|\mathcal{T}|\phi_{\epsilon,\alpha}(2)\varphi_{\mathbf{k}_0}(1)\rangle. \tag{22}$$

In physical terms f, the direct-scattering amplitude, can be interpreted as a measure for the probability that the projectile electron, labeled (1) and incident with wave vector $\mathbf{k}_0$, is scattered into the asymptotic (detector) state that is characterized by the wave vector $\mathbf{k}_1$ while the other electron (2) is being excited into the asymptotic state with the wave vector $\mathbf{k}_2$. Analogously, the exchange-scattering amplitude g describes the probability that electron (1) is scattered into the state $\mathbf{k}_2$ while particle (2) is promoted to the state with the wave vector $\mathbf{k}_1$.

If k_0 and k_1 are very large (with respect to the Fermi wave vector) and if a small amount of momentum is being transferred to the sample during the collision, it can be expected intuitively that $|f|\gg|g|$, i.e., the fast incoming electron is the one electron which emerges swiftly. In other words, in this case the electrons are distinguishable via their highly asymmetric energies and hence, as shown below, the spin asymmetry vanishes in this case.

From Eqs. (20) and (18) we deduce the relations

$$X^{(S=0)}(\mathbf{k}_1,\mathbf{k}_2;\mathbf{k}_0,\alpha)=C|f+g|^2, \tag{23}$$

$$X^{(S=1)}(\mathbf{k}_1,\mathbf{k}_2;\mathbf{k}_0,\alpha)=C|f-g|^2. \tag{24}$$

Equation (18) yields a relation that links the single-electron spin-resolved cross section $\mathcal{F}(m_{s_1},m_{s_2})$ with the triplet and singlet cross sections, namely,

$$\mathcal{F}(\uparrow,\Uparrow)=\mathcal{F}(\downarrow,\Downarrow)=X^{(S=1)}=C|f-g|^2, \tag{25}$$

$$\mathcal{F}(\downarrow,\Uparrow)=\mathcal{F}(\uparrow,\Downarrow)=\frac{1}{2}[X^{(S=1)}+X^{(S=0)}]=C|f|^2+C|g|^2. \tag{26}$$

Equations (16) and (17) reexpressed in terms of the singlet and the triplet partial cross sections, $X^{(S=0)}$ and $X^{(S=1)}$, read

$$\Lambda^{1,1}_{0,0}=\frac{1}{2}[X^{(S=1)}(\mathbf{k}_1,\mathbf{k}_2;\mathbf{k}_0;\alpha)-X^{(S=0)}(\mathbf{k}_1,\mathbf{k}_2;\mathbf{k}_0,\alpha)], \tag{27}$$

$$\Lambda^{0,0}_{0,0}=\frac{1}{2}[3X^{(S=1)}(\mathbf{k}_1,\mathbf{k}_2;\mathbf{k}_0,\alpha)+X^{(S=0)}(\mathbf{k}_1,\mathbf{k}_2;\mathbf{k}_0,\alpha)] =:2X_{av}. \tag{28}$$

Evidently, these two equations can as well be expressed in terms of the direct- and exchange-scattering amplitudes f and g. In Eq. (28) we introduced the spin-averaged cross section X_{av}.

B. Calculational scheme

For perfect clean surfaces the average over α in Eq. (14) implies summation over the surface Bloch wave vector $\mathbf{q}_\parallel$ and over the surface layers. The Bloch theorem for two interacting particles imposes a conservation law [cf. Eq. (2)] for the surface components of the *total* wave vector of the emitted electrons $\mathbf{K}_\parallel^+ = \mathbf{k}_{1\parallel} + \mathbf{k}_{2\parallel}$,[11] i.e., the change of $\mathbf{K}_\parallel^+$ from its initial value $\mathbf{k}_{0\parallel} + \mathbf{q}_\parallel$ (before the collision) is restricted to a multiple of the surface reciprocal-lattice vector $\mathbf{g}_\parallel$. This fact can be used to perform the integrals over $\mathbf{q}_\parallel$ in Eq. (14). Therefore, Eq. (14) reduces to a summation over the surface layers, indexed by l, and over $\mathbf{g}_\parallel$, i.e.,

$$W \propto \sum_{\mathbf{g}_\parallel, l} \{2X_{av}(\mathbf{k}_1, \mathbf{k}_2; \mathbf{k}_0, \mathbf{g}_\parallel, l)[\rho_{00}\overline{\rho}_{00}(\epsilon, \mathbf{\Lambda}_\parallel, l) - \rho_{10}\overline{\rho}_{10}(\epsilon, \mathbf{\Lambda}_\parallel, l) A^s(\mathbf{k}_1, \mathbf{k}_2; \mathbf{k}_0, \mathbf{g}_\parallel, l)]\delta(E_f - E_i)\}, \tag{29}$$

where

$$\mathbf{\Lambda}_\parallel = \mathbf{K}_\parallel^+ - \mathbf{g}_\parallel - \mathbf{k}_{0\parallel}. \tag{30}$$

We recall that spin interactions in the transition operator $\mathcal{T}$ have been neglected, in which case the parameters $\Lambda_{0,0}^{0,1}$ and $\Lambda_{0,0}^{1,0}$ vanish identically. In Eq. (29) we introduced the ''exchange-scattering asymmetry'' as

$$A^s := \frac{X^{(S=0)}(\mathbf{k}_1, \mathbf{k}_2; \mathbf{k}_0, \mathbf{g}_\parallel, l) - X^{(S=1)}(\mathbf{k}_1, \mathbf{k}_2; \mathbf{k}_0, \mathbf{g}_\parallel, l)}{X^{(S=0)}(\mathbf{k}_1, \mathbf{k}_2; \mathbf{k}_0, \mathbf{g}_\parallel, l) + 3X^{(S=1)}(\mathbf{k}_1, \mathbf{k}_2; \mathbf{k}_0, \mathbf{g}_\parallel, l)} = \frac{|f||g|\cos\delta}{|f|^2 + |g|^2 - |f||g|\cos\delta}. \tag{31}$$

In the last equation we reexpressed the cross sections in terms of the direct- $[f = f(\mathbf{k}_1, \mathbf{k}_2; \mathbf{k}_0, \mathbf{g}_\parallel, l)]$ and the exchange- $[g = g(\mathbf{k}_1, \mathbf{k}_2; \mathbf{k}_0, \mathbf{g}_\parallel, l)]$ scattering amplitudes and their relative phase δ. Thus, Eq. (31) reveals the spin asymmetry as the result of a quantum interference of the two amplitudes f and g.

Two conclusions follow directly from Eq. (31): (i) For a given layer the asymmetry A^s assumes unity value if $X^{(S=1)} = 0$. As stated above this is the case if the experiment is invariant under an exchange of $\mathbf{k}_1$ and $\mathbf{k}_2$. The function A^s varies between 1 and $-1/3$. The experimentally relevant quantity is, however, the value A^s weighted with the pair-emission cross section X_{av} [cf. Eqs. (29) and (34)], i.e., in cases where the cross section diminishes, e.g., for emission from atomic layers whose positions with respect to the surface are beyond the electron's inelastic mean free path, the pair-emission cross section and the spin asymmetry are not measurable (in the way proposed in this paper). (ii) In the cases $|f| \gg |g|$, $|f| \ll |g|$, or $f \perp g$ the spin asymmetry vanishes as the interference between f and g is then negligible.

To calculate the terms in Eq. (29) the state multipoles ρ_{10} and $\overline{\rho}_{10}$ are needed. These can be obtained by inverting the relations (9) and (10) as

$$\rho_{pq} = \sum_{m_s} (-)^{p-s-m_s} \langle s - m_s; s m_s | p q \rangle \rho^s_{m_s m_s}. \tag{32}$$

From this equation it is clear that even for pure states (fully spin-polarized states) all state multipoles are generally finite.

Since we have neglected spin-dependent interactions only the multipoles ρ_{00}, ρ_{01}, $\overline{\rho}_{00}$, and $\overline{\rho}_{01}$ are required. From Eqs. (9), (10), and (32) we deduce $\rho_{00}\overline{\rho}_{00} = [w_0(\mathbf{q}_\parallel, l, \epsilon)]/2$ and $\rho_{10}\overline{\rho}_{10} = [w_0(\mathbf{q}_\parallel, l, \epsilon)]P_1P_2/2$. Equation (29) can thus be written in the form

$$W \propto \sum_{\mathbf{g}_\parallel, l} w_0(\mathbf{\Lambda}_\parallel, l, \epsilon) X_{av}[1 + \mathcal{A}]\delta(E_f - E_i), \tag{33}$$

where the asymmetry function $\mathcal{A}$ is defined by the relation

$$\mathcal{A} = P_1 \frac{\sum_l [w(\mathbf{\Lambda}_\parallel, l, \epsilon, \Downarrow) - w(\mathbf{\Lambda}_\parallel, l, \epsilon, \Uparrow)] \sum_{\mathbf{g}_\parallel} X_{av} A^s \delta(E_f - E_i)}{\sum_{l'} w_0(\mathbf{\Lambda}_\parallel, l', \epsilon) \sum_{\mathbf{g}'_\parallel} X_{av} \delta(E_f - E_i)} = \frac{W(\uparrow\Uparrow) - W(\downarrow\Uparrow)}{W(\uparrow\Uparrow) + W(\downarrow\Uparrow)}. \tag{34}$$

This result for the asymmetry admits a simple structure in some limiting situations:

For atomic gaseous targets the sample's polarization vector $\mathbf{P}_2$ is a constant, experimentally determined quantity, namely, the polarization P_a of the atomic beam. Therefore, $\mathcal{A}$ reduces to $\mathcal{A} = P_a P_e A^{(s)}$.

For a spin-polarized homogeneous electron gas (Stoner model) P_2 is directly related to the density of states $\rho_{\Uparrow,\Downarrow}$ and therefore $\mathcal{A} = P_1[(\rho_\Downarrow - \rho_\Uparrow)/(\rho_\Downarrow + \rho_\Uparrow)]A^{(s)}$.

For bulk sensitive studies, e.g., for a high-energy electron beam ($E_0 > 1$ keV), the three-dimensional translational symmetry of the sample results in a simplified form of Eq. (34), namely,

$$\mathcal{A} = P_1 P_2 \frac{\sum_{\mathbf{g}} X_{av} A^s \delta(E_f - E_i)}{\sum_{\mathbf{g}'} X_{av} \delta(E_f - E_i)}. \tag{35}$$

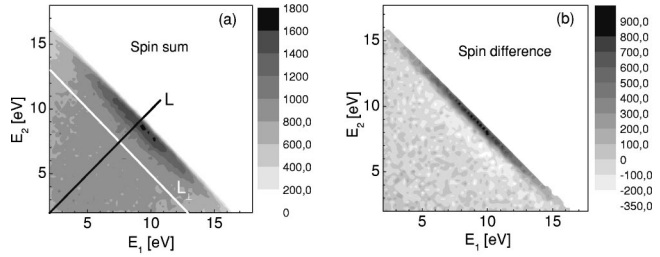

FIG. 2. (a) The coincident two-electron spectrum measured in the geometry of Fig. 1. The incident energy is $E_0=22.6$ eV and the data are summed for two polarizations of the incoming electron beam. The data set was integrated over the whole area of the detectors, therefore the emission angles are determined within the range $\theta_1=40°\pm15°$ and $\theta_2=40°\pm15°$. Along the line L, the two electrons escape with equal energies. Along the lines perpendicular to L the electron pairs have a constant total energy $E_{\rm tot}=E_1+E_2$ $=$const. The absolute values of the spectra are not determined whereas the absolute magnitude and the sign of the spin asymmetry is measured. (b) The difference between two spectra obtained when $\mathbf{P}_1$ is parallel to $\hat{\mathbf{M}}$ and $\mathbf{P}_1$ is antiparallel to $\hat{\mathbf{M}}$.

Here $\mathbf{g}$ is a three-dimensional reciprocal-lattice vector and the polarization vector P_2 is given by $P_2=[w(\mathbf{\Lambda},\epsilon,\Downarrow)$ $-w(\mathbf{\Lambda},\epsilon,\Uparrow)]/[w_0(\mathbf{\Lambda},\epsilon)]$. In this context it should be noted that, except for some highly symmetric situations, in the high-energy regime A^s might be very small due to the dominance of direct scattering.

IV. COMPARATIVE ANALYSIS OF EXPERIMENTAL AND THEORETICAL RESULTS

We conducted the experiment for a series of impact energies from $E_0=20$ eV up to $E_0=37.6$ eV in the geometry shown in Fig. 1. The two-dimensional distributions of coincidence events for $E_0=22.6$ eV are shown in Fig. 2(a) as a function of the energies of the two electrons E_1 and E_2. In this graph, the two data sets obtained with different electron-beam polarizations with respect to the sample magnetization are summed up. We recall that the emission angles θ_1 and θ_2 are also measured, however, the data depicted in Fig. 2 are integrated over the whole solid angle of detection. The position of the Fermi level E_F is shown as well as the line L along which the two electrons have equal energies. Figure 2(b) shows the difference in the spectrum associated with reversal of the spin polarization of the electron beam. Equivalently, one can also plot the electrons' energy dependence of the asymmetry $\mathcal{A}$. The line L is of a special importance as it corresponds to the Γ point for $\theta_1=\theta_2$, as can be seen from Eq. (2) $[\mathbf{k}_{0\|}=0,\mathbf{k}_{1\|}=-\mathbf{k}_{2\|}]$. Different points on L correspond to different binding energies ϵ of the conduction-band electrons [cf. Eq. (1)]. On the other hand, in the highly symmetric geometry of the setup shown in Fig. 1 and along the line L $(E_1=E_2)$ the complete experiment and in particular the sample's properties are invariant under a 180° rotation with respect to the $z\|\mathbf{k}_0$ direction. Such a symmetry operation is, however, equivalent to an exchange of $\mathbf{k}_1$ and $\mathbf{k}_2$. Therefore, along the line L in Figs. 2(a) and 2(b) the triplet scattering vanishes [cf. Eqs. (20)–(22) and (24)] and therefore the term A^s (31) becomes unity. This means that the spin asymmetry $\mathcal{A}$ (34) in this situation reflects the properties of the electronic band structure of the sample. The scattering dynamics plays no role due to symmetry (as far as the quantity $\mathcal{A}$ is concerned).

The above statements apply strictly speaking along the line L only. In our experiment, however, we have to integrate over a finite detection solid angle in order to obtain reasonable statistics, i.e., in the geometry of Fig. 1 and along the line L the electrons are emitted into a solid angle Ω_θ with an aperture Δ_θ. The sampling over Ω_θ implies an averaging over $\hat{\mathbf{k}}_1$ and $\hat{\mathbf{k}}_2$ within a certain range. From Eq. (2) it follows that this procedure corresponds to an integration in a certain region in the Brillouin zone around the Γ point. It should be stressed, however, that in the case of a finite angular resolution the coincident signal cannot be directly related to the sample's electronic structure since the triplet scattering is then generally finite and the term A^s [Eq. (31)] is not simply a constant (except for $\theta_1=\theta_2$, $E_1=E_2$ where $A^s=1$). The quantitative shape of A^s away from the highly symmetric points $\theta_1=\theta_2$ and $E_1=E_2$ is strongly dependent on the scattering dynamics (embedded in $\Lambda^{p_1,p_2}_{q_1,q_2}$) whose modeling poses a real challenge, even for simple few-body systems.[16,17]

The asymmetry A^s has its unity maximum value at θ_1 $=\theta_2$ and $E_1=E_2$. Thus, any angular sampling (Δ_θ) will decrease the unity value of A^s. This argument is, however, not valid for $\mathcal{A}$, since the angular integration procedure involves different electronic states of the conduction band whose spin polarization is not known *a priori* and depends on the material under investigation. For the present case we observed in the theoretical results that angular integration reduces the values of the spin asymmetries $\mathcal{A}$.

In Fig. 3 we assess the above statements by contrasting theoretical with experimental spectra along the line L in Fig. 2. In Figs. 3(a)–3(c) the angular integration for each of the TOF detectors is $\Delta_\theta=15°$ whereas in Figs. 3(a′)–3(c′) the angular integration is decreased to $\Delta_\theta=7.5°$. In all cases the angular resolution is accounted for by the theory. As stated above for the strict conditions $\theta_1=\theta_2$ and $E_1=E_2$ the spin asymmetry $\mathcal{A}$ [Eq. (34)] is an image of the spin polarization P_2 [cf. Eq. (6)] at the respective point in the Brillouin zone. Therefore, the value of $\mathcal{A}$ should not depend on the incident energy E_0 of the beam (since P_2 is independent of E_0). For the theoretical results we observe the general trend that the finite angular resolution has the effect of decreasing the value $\mathcal{A}$ {due to the decreased value of A^s [Eq. (31)], as explained above}. Improving on the angular resolution $[\Delta_\theta$ $=15°$ in Figs. 3(a)–3(c) and $\Delta_\theta=7.5°$ in Figs. 3(a′)–3(c′)] increases the averaged value of A^s and possibly enhances the value of $\mathcal{A}$. These expectations are basically confirmed by the theoretical results in the region around the Fermi level (1 eV below E_F) (cf. Fig. 3): The theoretical $\mathcal{A}$ increases substantially when the angular resolution is improved and the value and sign of $\mathcal{A}$ do not depend on E_0 near the Fermi energy. While the agreement between theory and experiment can be regarded as satisfactory up to 2 eV below E_F, large deviations are observed for the electron-pair emission from levels deeper in the band. For these levels the experimental

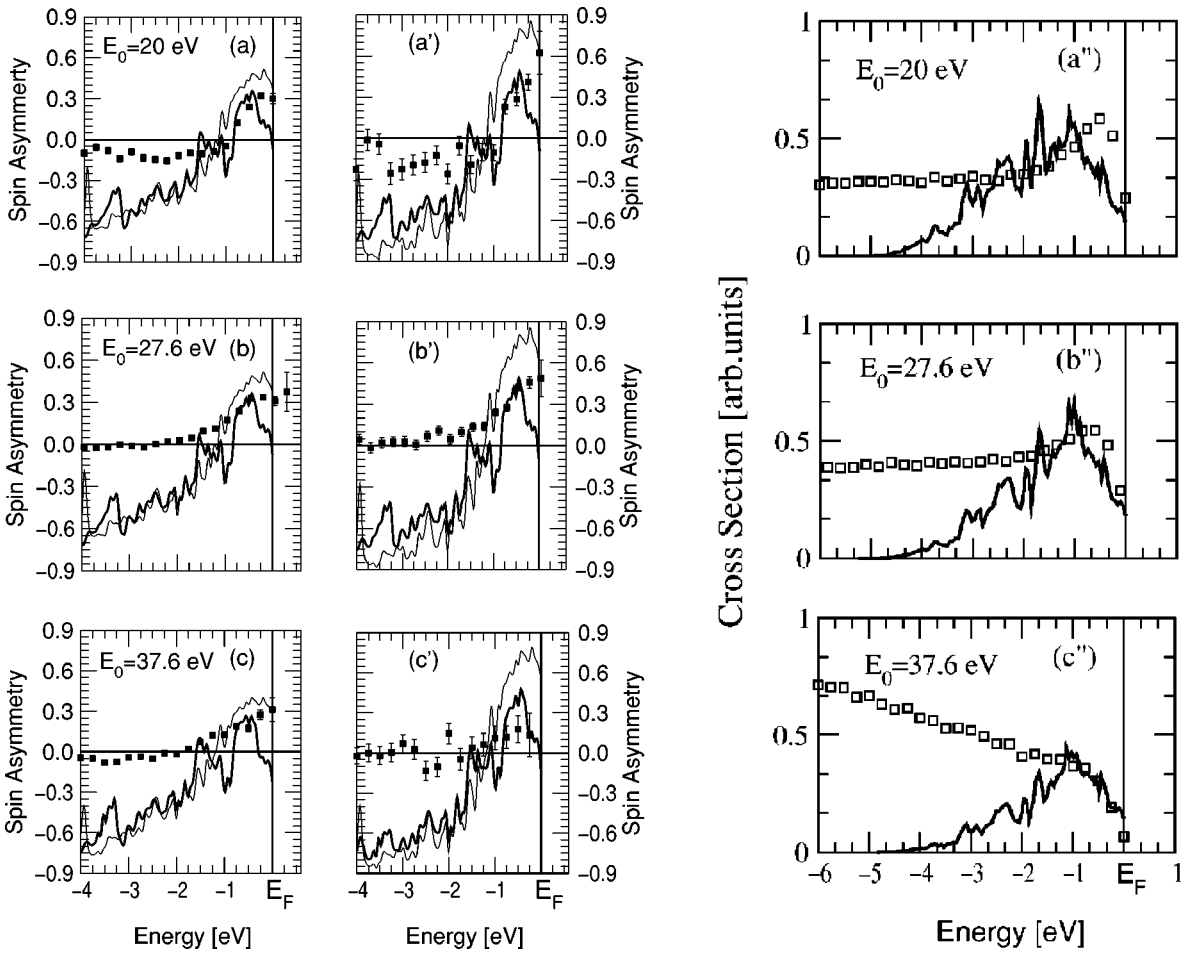

FIG. 3. With the same geometry as in Figs. 1 and 2 we scan the spin asymmetry $\mathcal{A}$ in the electron-pair-emission cross section along the line of equal energies of the electrons, i.e., along the line labeled L in Fig. 2(a). The asymmetry $\mathcal{A}$ is plotted as a function of the energy $\epsilon = E_{\rm tot} - E_0$. According to Eq. (1) ϵ corresponds to the binding energy of the ground-state electrons and hence the Fermi energy is at $\epsilon = 0$. The sets (a)–(c) and (a″)–(c″) show, respectively, the spin asymmetry in the electron-pair spectrum and the spin-averaged spectrum for three different incident energies E_0 of the incoming electrons [$E_0 = 20$ eV in (a), (a′), and (a″), $E_0 = 27.6$ eV in (b), (b′), and (b″), and $E_0 = 23.6$ eV in (c), (c′), and (c″)]. In (a)–(c) and (a″)–(c″) the angular integration for each of the detectors is $\theta_{1/2} = (40 \pm 15)°$, whereas in (a′)–(c′) the solid angle of the integration area was restricted to $\theta_{1/2} = (40 \pm 7.5)°$. Full squares with error bars are experimental data whereas the solid lines are the theoretical results.

results are also different for different incident energies E_0 and therefore they cannot be related directly to the ground-state electronic band structure. To get insight into the origin of these discrepancies we discuss the main limitations of our theoretical approach: In the present theory, when we derive the single-particle Green function, we do not employ a proper expression for the self-energy operator which would generally have the effect of (a lifetime) broadening and an energetic shifting of the quasiparticle states.[18] In our calculations we assume the imaginary part of the self-energy to be merely a spin-independent constant (0.02 eV). Therefore, our theory yields an energetic spreading of the bound states which is very narrow. For a given Bloch wave vector, when we energy-scan the Brillouin zone, e.g., as is done in Fig. 3, we encounter only narrow states centered around specific energies, and hence we see the spiky structure of the theoretical curves shown in Fig. 3 (note, however, that in Fig. 3 we accounted for the finite experimental angular resolution which results in a certain broadening of the peaks). An additional shortcoming of the present theory is that we do not account for a dynamic, multiple inelastic scattering of the electron pair from other electrons in the sample (the electron-electron scattering within the electron pair is treated properly). This is justifiable when the emission of the electron pair is from states around the Fermi level, for the energy conservation (1) pins down the energetic position of the bound electron [$\epsilon = (E_1 + E_2) - E_0$]. For states deep in the band this determination of the initial binding energy of the ejected electrons is no longer unique. This is because, on their way out to the vacuum, the excited electrons may scatter inelastically from other target electrons which further propagate in the sample and remain undetected. This leads to a spin decoherence of the excited electrons since, as we have shown in this paper, the electron-electron inelastic scattering is strongly spin dependent (due to the exchange coupling).

These statements are in line with the behavior of the experimental and theoretical results shown in Figs. 3(a)–3(c)

and Figs. 3(a″)–3(c″). In the latter figures the spin-averaged electron-emission rate corresponding to the geometry of Figs. 3(a)–3(c) is depicted. In contrast to theory, the experiments show a considerable increase in the coincidence rate for very low electron energies, i.e., for large negative initial binding energies [$\epsilon=(E_1+E_2)-E_0$]. In fact the extent of the experimental spectra [not fully shown in Figs. 3(a″)–3(c″)] goes beyond the conduction bandwidth. On the other hand these slow electrons might have been originally fast (at the time of their creation) and suffered one or more inelastic electronic collisions before escaping into the vacuum. This additional channel, not accounted for theoretically, leads to an increase in the cross sections for the emission of two slow electrons (or from levels deep in the band). Due to the spin decoherence associated with these inelastic processes the spin asymmetry, as shown in Figs. 3(a)–3(c), diminishes when the contribution of such inelastically scattered electron pairs becomes a sizable part of the recorded coincidence spectra. This argument gains support by correlating the behavior of the experiments in Figs. 3(a)–3(c) and Figs. 3(a″)–3(c″), e.g., with increasing impact energy E_0 the contribution of the inelastic, energy-loss processes of the electron pairs increases, while in this case the spin asymmetry decreases. As expected, the theory shows hardly a dependence on E_0 of the spectra in Figs. 3(a) and 3(c″).

In Fig. 2 we highlighted the importance of the equal-energy line L and showed in Fig. 3 the electron-pair spectrum along L. For events along this line, the binding energy ϵ of valence electron removed from the Γ point varies. If we consider lines $L_\perp$ in Fig. 2 which are perpendicular to L, we consider events at fixed binding energy ϵ [this is because in this case $E_{\rm tot}=E_1+E_2$ is constant and due to Eq. (1), $\epsilon=E_{\rm tot}-E_0$]. The electron-pair spectrum along $L_\perp$ is an energy pair-correlation function. It is a measure of the probability that the first electron will escape with energy E_1 and the other electron will emerge with energy $E_2=E_{\rm tot}-E_1$. This probability will strongly depend on the strength of the correlation between these two electrons. In particular, the spin asymmetry in this spectrum is intimately related to the strength of the exchange interaction as quantified by the amplitude g [Eq. (22)]. If g vanishes (distinguishable electrons) the spin asymmetry diminishes. Therefore it is of interest to analyze $\mathcal{A}$ along the line $L_\perp$, as done in Fig. 4 for three different total energies of the electron pair for a fixed incident energy $E_0=22.6$ eV. When the two electrons escape with equal energies $E_1=E_2$ (the crossing point of the lines $L_\perp$ and L) the triplet scattering $X^{(S=1)}$ vanishes, as explained above. Therefore, for $E_1=E_2$ we obtain $A^{(s)}=1$. In this situation ($E_1=E_2$), the *magnitude* and *sign* of the asymmetry $\mathcal{A}$ are dictated merely by $P_2(\epsilon)$. Since $P_2(\epsilon)$ may be positive or negative, $\mathcal{A}$ may have a different sign depending on $E_{\rm tot}$ (or on $\epsilon=E_{\rm tot}-E_0$). In general, the shape of $\mathcal{A}$ as depicted in Fig. 4 can be understood from the following arguments emerging from the analysis of our theoretical results: For $E_1=E_2$, the triplet cross section vanishes, and therefore $A^{(s)}$ reaches its highest value (unity). This structure is at a peak (minimum) when $P_2>0$ ($P_2<0$). The decrease in $\mathcal{A}$ for $E_1>E_2$ or $E_2<E_1$ is due to a dominance of the direct-scattering amplitude $|f|$ over the exchange amplitude $|g|$,

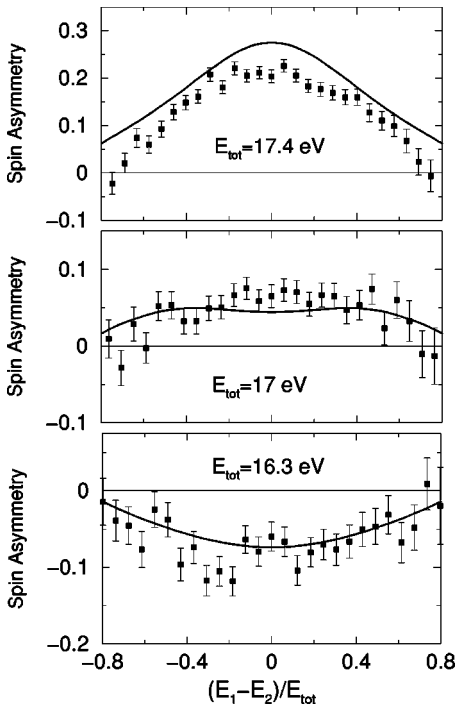

FIG. 4. For a fixed total energy $E_{\rm tot}$ and a fixed energy $\epsilon=E_{\rm tot}-E_0$ of the initially bound electron we measure (full squares) and calculate (solid lines) the spin asymmetry $\mathcal{A}$ (34) as a function of the energy sharing of $E_{\rm tot}$ between the two emitted electrons. The zero point indicates the position of equal-energy sharing. Three sets are shown corresponding to three different values of $E_{\rm tot}$ as indicated in the figures. The experimental data are obtained from Fig. 2 by taking cuts along the lines perpendicular to L, the position marking equal energies. Theoretical results have been averaged over the solid angle, as stated in Fig. 2.

i.e., it is more likely that the fast incoming electron will escape as the fast electron than it is for it to lose almost all its energy and emerge as the slow one. As deduced above, $\lim_{(|g|/|f|)\to 0}A^{(s)}=(|f||g|\cos\delta)/(|f|^2|g|^2-|f||g|\cos\delta)\to 0$, and hence the asymmetry in Fig. 4 decreases with increasing deviation from $E_1=E_2$.

V. CONCLUSIONS

In this work we presented a theoretical and experimental analysis of the correlated electron-pair emission from magnetic surfaces induced by the impact of polarized electrons. We employed a tensorial symmetry analysis to disentangle geometrical from dynamical properties and to classify the spectra according to their symmetry properties. We also described a calculational model for the two-particle spectrum and performed numerical calculations using a realistic electronic band structure of the sample. Under certain conditions worked out in this study, the present two-particle coincidence technique allows for an insight into the spin-split electronic band structure of the sample and is also suitable to investigate the electrons' exchange scattering at surfaces.

ACKNOWLEDGMENTS

The technical assistance of H. Schwabe and A. Wiessner is gratefully acknowledged.

[1] J. Kirschner, D. Rebenstorff, and H. Ibach, Phys. Rev. Lett. **53**, 698 (1984).
[2] M. Plihal, D. L. Mills, and J. Kirschner, Phys. Rev. Lett. **82**, 2579 (1999).
[3] D. L. Abraham and H. Hopster, Phys. Rev. Lett. **62**, 1157 (1989).
[4] H. Ibach and D. L. Mills, *Electron Energy Loss Spectroscopy and Surface Vibrations* (Academic Press, New York, 1982).
[5] *Polarized Electrons in Surface Physics*, edited by R. Feder (World Scientific, Singapore, 1985).
[6] J. Berakdar, Phys. Rev. Lett. **83**, 5150 (1999).
[7] S. N. Samarin, J. Berakdar, O. Artamonov, and J. Kirschner, Phys. Rev. Lett. **85**, 1746 (2000).
[8] S. Samarin, O. Artamonov, J. Berakdar, A. Morozov, and J. Kirschner, Surf. Sci. **482**, 618 (2001).
[9] P. Blaha, K. Schwarz, P. Sorantin, and S. B. Trickey, Comput. Phys. Commun. **59**, 399 (1990); X. Qian and W. Hübner, Phys. Rev. B **60**, 16 192 (1999).
[10] E. Tamura, in *Application of Multiple Scattering Theory to Materials Science*, edited by W. H. Butler, P. H. Dederichs, A. Gonis, and R. L. Weaver, Mater. Res. Soc. Symp. Proc. No. 253 (Materials Research Society, Pittsburgh, 1992), p. 347.
[11] J. Berakdar, S. N. Samarin, R. Herrmann, and J. Kirschner, Phys. Rev. Lett. **81**, 3535 (1998).
[12] U. Fano, Rev. Mod. Phys. **29**, 76 (1957).
[13] D. M. Brink and G. R. Satchler, *Angular Momentum*, 3rd ed. (Clarendon Press, Oxford, 1994).
[14] H. Gollisch, X. Yi, T. Scheunemann, and R. Feder, Phys. Rev. B **60**, 8055 (1999).
[15] S. Samarin, O. Artamonov, A. Morozov, and J. Kirschner (unpublished).
[16] M. Streun, G. Baum, W. Blask, and J. Berakdar, Phys. Rev. A **59**, R4109 (1999).
[17] J. Lower, E. Weigold, J. Berakdar, and S. Mazevet, Phys. Rev. Lett. **86**, 624 (2001).
[18] L. Hedin, J. Phys. C **11**, R489 (1999); **11**, R528 (1999); P. Fulde, *Electron Correlation in Molecules and Solids*, Springer Series in Solid-State Sciences, Vol. 100 (Springer-Verlag, Berlin, 1991).